Electronic Supplementary Material (ESI) for ChemComm.

Supporting Information

Facile *in situ* synthesis of carbon quantum dots/graphene heterostructure as an efficient metal-free electrocatalyst for overall water splitting

Experimental

Chemicals and materials

Graphite powder (80 mesh) was purchased from Qingdao Graphite Company. Tetrabutylammonium hexafluorophosphate (TBAPF6, 99%, powder), N, N-dimethylformamide (DMF, ≥99%), were obtained from Sigma-Aldrich. Proprylene carbonate (PC, ≥99.9%) was purchased from aladdin.

Preparation of carbon quantum dots/graphene heterostructure

Graphite powder (30 mg) was put in a porous plastic tube with a platinum plate inserted as negative electrode, another platinum plate served as positive electrode. Both electrodes were immersed in proprylene carbonate (PC) with tetra- butylammoniumhexafluorophosphate (TBA PF_6; 0.1 M) and a voltage of 30 V was applied for 12 h. After the electrochemical expansion step, the mixture was transferred into 80 ml Teflon cup inserted in a stainless steel autoclave for solvothermal treatment at 170 °C for 12 h; After that, the samples was filtered washing with DMF solution for three times, then dried in a vacuum oven for 8 h at 60 ^{o}C. Finally, the samples were annealed at 300 ^{o}C to remove residue solvent in inert atmosphere for 30 min. The obtained sample was defined as G-EX-ST. Compared with G-EX-ST, G-EX (treatment only with electrochemical exfoliation from graphite powder), G-EX-300 (treatment only with electrochemical exfoliation from graphite powder and then annealed at 300 ^{o}C) and G-ST (treatment only with solvothernal treatment from graphite powder) were prepared.

Characterization

X-ray diffraction (XRD) analysis was carried out on an X-ray diffractometer (Ultima IV-185) with Cu Ka radiation. Raman spectra were recorded on a JobinYvonLabRAM HR800 micro-Raman spectrometer using a laser excitation of 632 nm at room temperature. X-ray photoelectron spectroscopy (XPS) was performed on Thermo Fisher SCIENTIFIC using Al Ka X- ray source. The morphologies of the samples were investigated by transmission electron microscopy (TEM, FEI Tecnai F20) and scanning electron microscopy (SEM, JSM-7001F). Fourier transform infrared (FTIR) spectra were recorded using a Bruker spectrometer. The height of the material was

obtained by Atomic Force Microscope (Agilent 5500) instrument.

Electrochemical tests

All the electrochemical measurements were carried out on a CHI 660E electrochemical workstation (CH Instruments, Inc., Shanghai) with a standard three-electrode setup. A glassy carbon electrode (GCE, 3 mm in diameter) used as the support for the working electrode. Immobilization of sample was achieved by drop-casting 5 ul sample (5mg sample and 20 μL Nafion solution were dispersed in 1 ml water-ethanol solution with volume ratio of 3:1) onto GC working electrodes. Hg/HgO and a platinum plate were used as reference and counter electrode, respectively. The HER performance was evaluated in N_2-saturated 1 M KOH solution, respectively. The OER performance was evaluated in O_2-saturated 1 M KOH solution. The electrocatalytic activity of the samples was examined by obtaining polarization curves using linear sweep voltammetry (LSV) with a scan rate of 5 $mV \cdot s^{-1}$ at room temperature. The electrochemical impedance spectroscopy (EIS) was carried out on an IM6e electrochemical workstation over a frequency range from 10^5 to 1 Hz with a 5 mV amplitude. The stability measurements were performed by cyclic voltanmmetry scanning 2000 cycles (CV, sweep rate, 50 $mV \cdot s^{-1}$) and long-term chronoamperometry. CV method also was used to determine the electrochemical double-layer capacitances (C_{dl}). Electrochemically active surface area could be evaluated from the slope of the plot of the charging current versus the scan rate, which was directly proportional to C_{dl}. Here, in the HER and OER, both their potentials are referred to revisable hydrogen electrode (RHE) according to the following equation of $E_{RHE} = E_{Hg/HgO} + 0.059\ pH + E^{\theta}_{Hg/\ HgO}$, where E_{RHE} is the converted potential vs. RHE, $E_{Hg/\ HgO}$ is the experimental potential measured against the Hg/HgO.

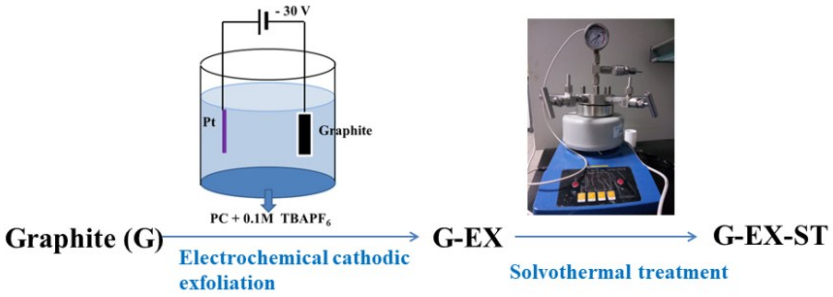

Scheme S1 The preparation process of CQDs/graphene heterostructures (abbreviated as G-EX-ST).

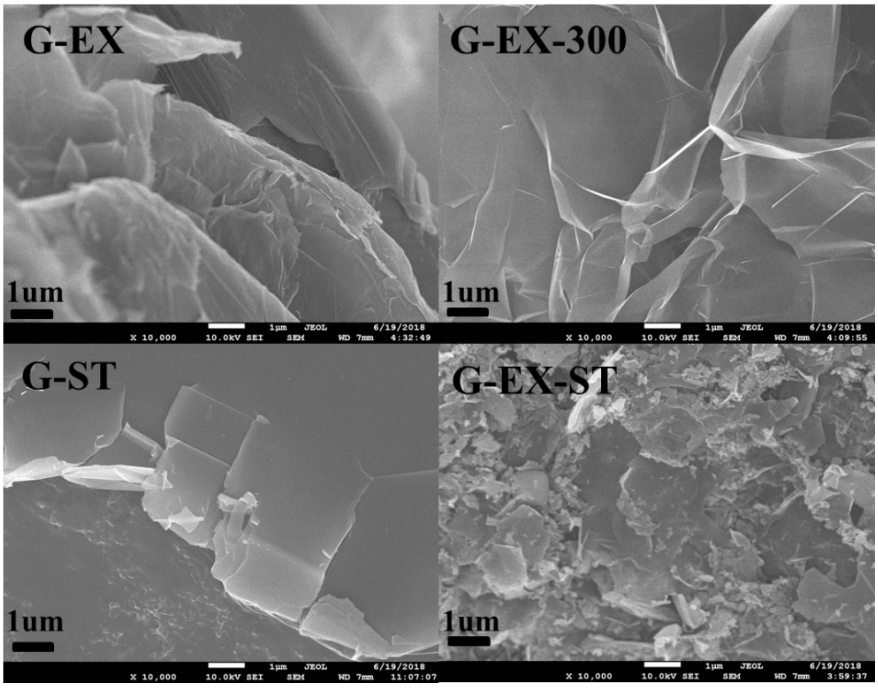

Fig. S1. SEM images of the G-EX, G-EX-300, G-ST and G-EX-ST. The flake size of G-EX-ST is much smaller.

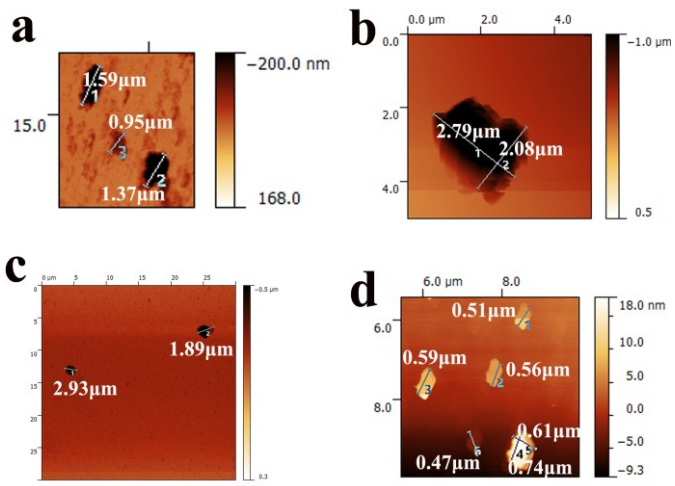

Fig. S2 AFM images of (a) G-EX, (b) G-EX-300, (c)G-ST and (d) G-EX-ST.

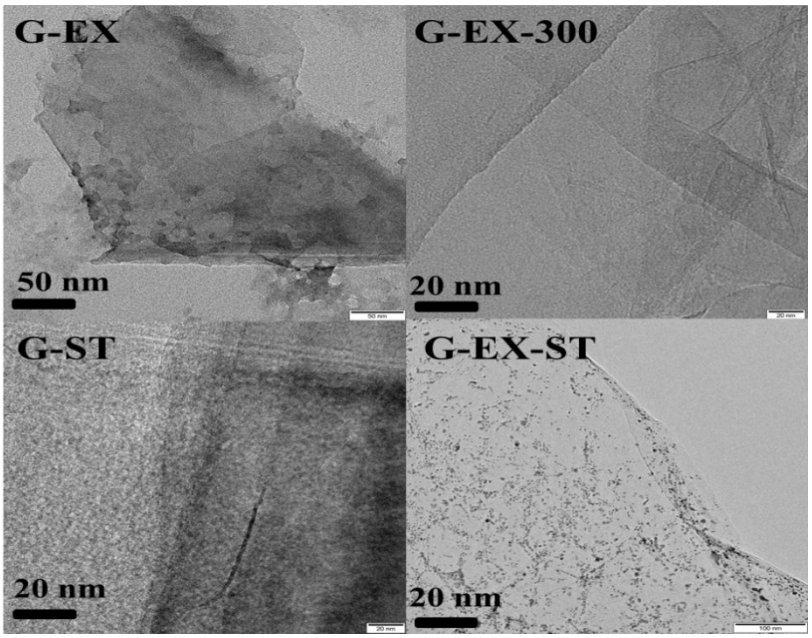

Fig. S3. TEM images of G-EX, G-EX-300, G-ST and G-EX-ST. Many quantum dots anchored on G-EX-ST, while no dots appeared on other samples.

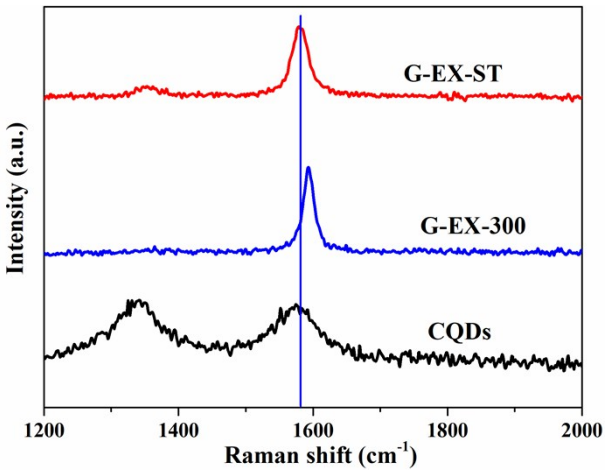

Fig. S4 Raman spectra of G-EX-ST (CQDs/grapheme composite), G-EX-300 (grapheme) and CQDs. The Raman (G) band of G-EX-ST (CQDs/graphene heterostructure) shows a slight, but noticeable up-shift with respect to those of the CQDs and down-shift to those of grapheme (G-EX-300). This results indicates a strong π-π stacking interaction between the CQDs and grapheme matrix

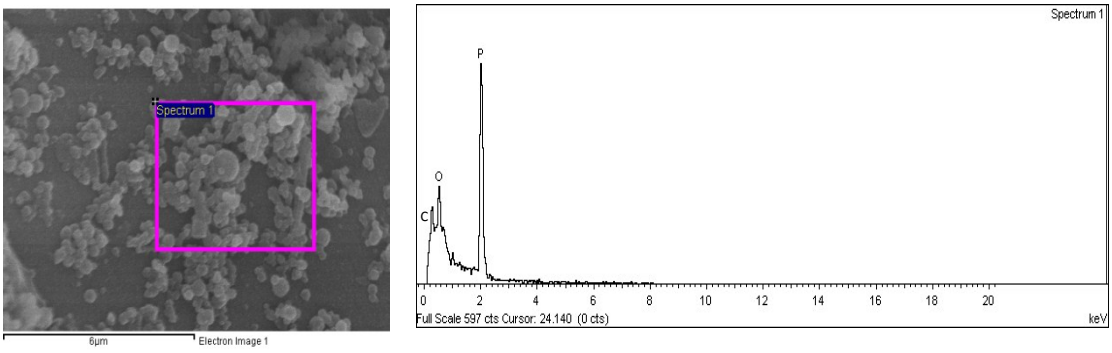

Fig. S5 SEM and corresponding point-resolved EDS spectrum of black phosphorous.

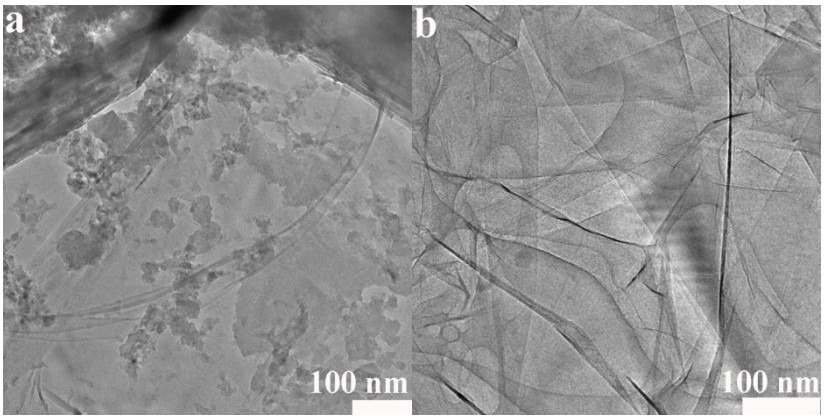

Fig. S6 TEM images of compared samples prepared through electrochemical exfoliation and then solvothermal treatment in (a) dimethylsulfoxide (DMSO) and (b) methylpyrrolidone (NMP). The TEM images showed that no quantum dots appeared over the samples prepared in DMSO solvent or NMP solvent. As for the sample in NMP solvent, no nanostructure material generated on the pure smooth grapheme sheets while the amorphous carbon formed over the sample prepared in DMSO. From above result, it's concluded that the PC solvent affected the formation of carbon quantum dots (CQDs) over G-EX-ST.

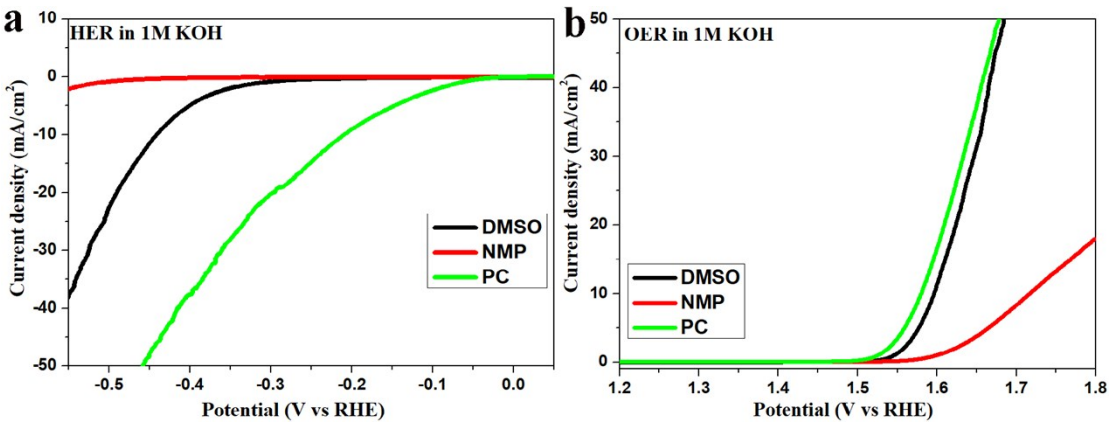

Fig. S7 LSV curves of compared samples prepared through electrochemical exfoliation and then solvothermal treatment in dimethylsulfoxide (DMSO) and methylpyrrolidone (NMP) for HER (a) and OER (b) in 1 M KOH with a scan rate of 5 $mV \cdot s^{-1}$ at room temperature, respectively. This result showed that the HER and OER activity of obtained samples prepared in different solvents are different as follows: PC > DMSO > NMP, suggesting that the influence of solvent on the electrochemical performance of resultant catalysts. Moreover, as for G-EX-ST sample, the PC solvent played important role in its activity.

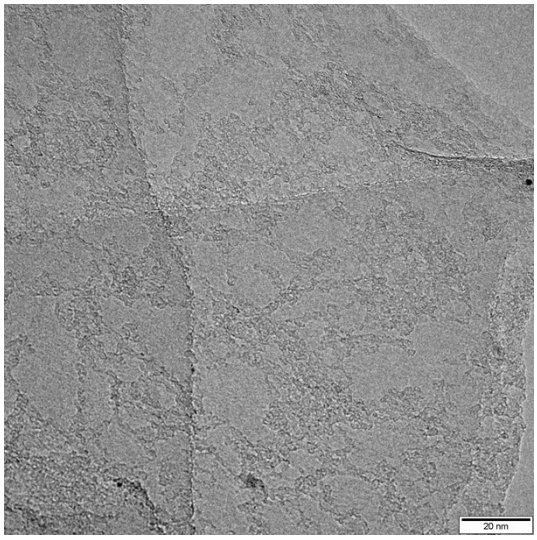

Fig. S8 TEM of the electrochemically exfoliated graphene nanosheets under solvothermal treatment in pure PC solution. Little CQDs attached to the graphene sheets, indicating CQDs didn't originate from pure original PC solvent or graphite but from electrochemically treated PC.

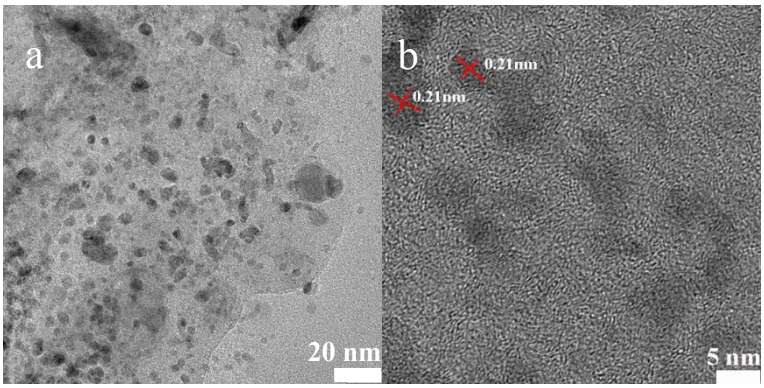

Fig. S9 TEM (a) and HRTEM (b) image of the obtained product originated from the obtained TBA PF_6 electrolyte solution after electrochemical exfoliation process underwent further solvothermal treatment. The lattice fringes with spacing of ~0.21nm ascribed to graphitic carbon (100), meaning the formation of carbon quantum dots.

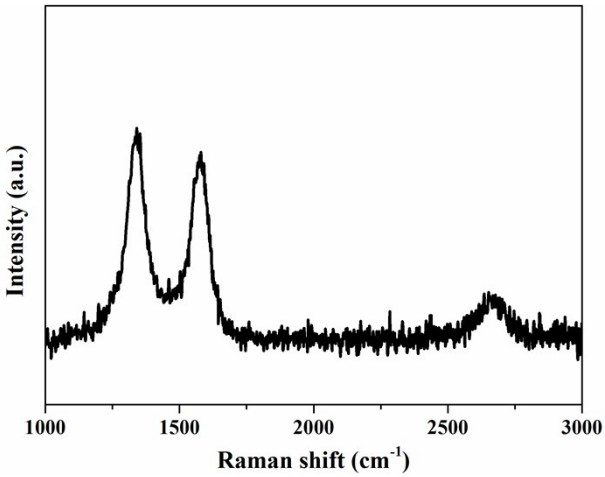

Fig. S10 Raman spectra of CQDs. The Raman spectra shows typical peaks for carbon materials with a sharp G peak located at 1580 cm^{-1} and an obvious D peak located at 1380 cm^{-1}. The large ratio of I_D/I_G (1.13) means that the CQDs are rich with defects.

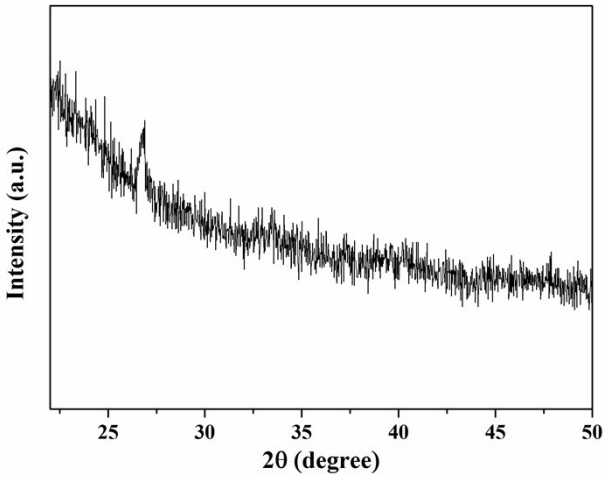

Fig. S11 XRD spectra of CQDs. The XRD spectrum also reveals a characteristic peak for graphitic carbon at 26.5 degree, corresponding to (002) facets.

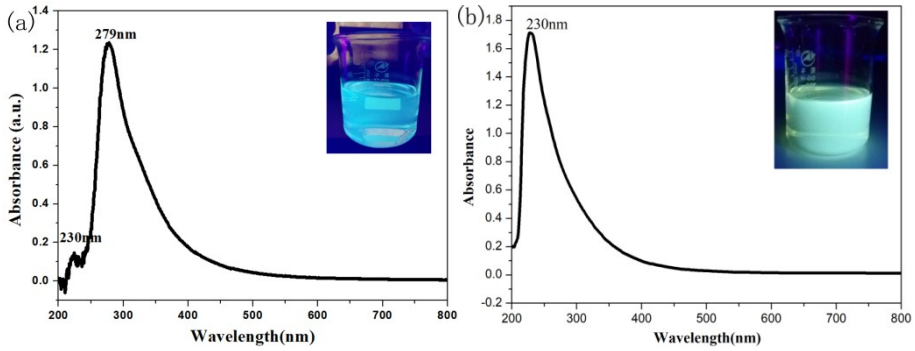

Fig. S12 UV-vis absorption of the obtained CQDs solution (a) and G-EX-ST (CQDs-Graphene composite) solution (b). insets are photographs of fluorescence phenomenon. The absorption peak at 230 nm can be attributed to the π–π* transition of aromatic sp^2 domains while the 280 nm absorption peak may be assignable to the existence of rich edges in CQDs or the n–π* transition of the functional group containing oxygen

Table S2. Comparison of selected state-of-the-art non-metal HER electrocatalysts in acidic/alkaline aqueous media

Catalysts	Electrolyte	Potential (V vs RHE)	Ref
C3N4@Graphene	0.5 M H2SO4	-0.219	1
C3N4@NG	0.5 M H2SO4	-0.24	2
Porous C3N4@NG 750 cycles	0.5 M H2SO4	-0.08	3
Bacterium derived carbon	0.5 M H2SO4	-0.20	4
Activated carbon	0.5 M H2SO4	-0.33	5
nitrogen-doped carbon nanotubes	0.1M NaOH	-0.34	6
Defective graphene	1 M KOH	-0.32	7
N, P and O tri-doped porous graphite carbon@oxidized carbon cloth	1 M KOH	-0.45	8
CQDs-graphene	1 M KOH	-0.194	This work

Table S3. Comparison of selected state-of-the-art non-metal OER electrocatalysts in alkaline aqueous media Catalysts

catalysts	Electrolyte	Potential (V vs RHE)	Ref
oxidized carbon cloth	0.1 M KOH	1.71	9
g-C3N4 –CNT	0.1 M KOH	1.60	10
oxygen-functionalized graphene	1.0 M KOH	1.68	11
N and P co-doped mesoporous nano carbon	0.1 M KOH	1.58	12
N-doped carbon nanocages	0.1 M NaOH	1.69	13
Nitrogen-doped carbon	0.1 M KOH	1.61	14
Defective graphene	1.0 M KOH	1.57	7
N, P and O tri-doped porous graphite carbon@oxidized carbon cloth	1.0 M KOH	1.64	8
CQDs-graphene	1.0 M KOH	1.58	This work

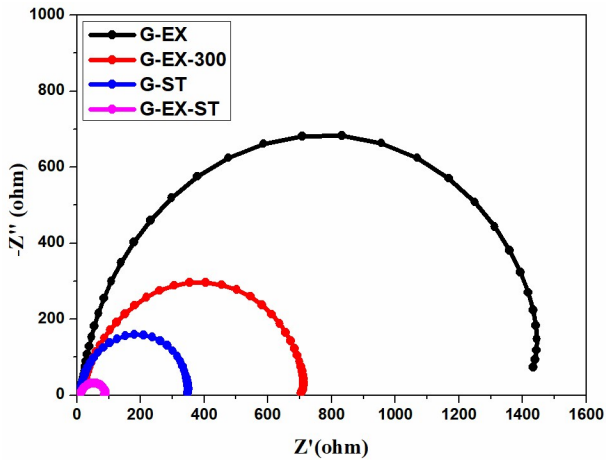

Fig. S13 EIS curves of the G-EX-ST and the compared samples in 1.0 M KOH solution.

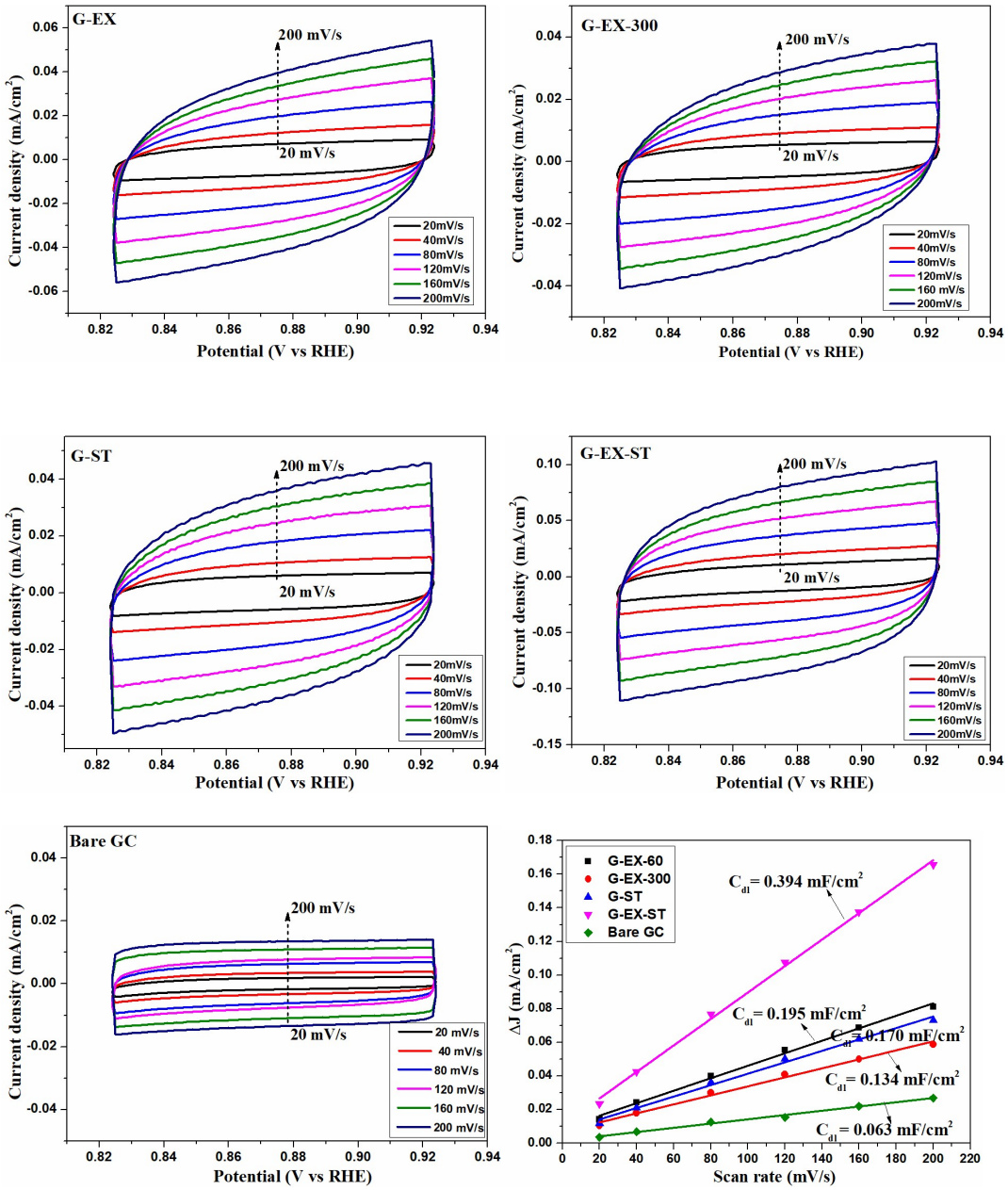

Fig. S14 Cyclic voltammograms of G-EX, G-EX-300, G-ST and G-EX-ST based films at scan rates from 20 to 200 mV s^{-1} in 0.5 M H_2SO_4. For all catalysts, only capacitive currents are observed. The differences in current density variation ($\Delta J=J_a-J_c$) at an overpotential of 0.875 V plotted against the scan rate fitted to a linear regression enables the estimation of C_{dl}. After extracting the Cdl from the fitted linear regressions, we cancalculated the electrochemically active surface area (EASA) from the equation of EASA $=C_{dl}/C_s$, where Cs are assumed to be same for all electrodes. Thus, the variation trend of EASA is in line with that of C_{dl}.

EASA $_{G\text{-}EX\text{-}ST}$ (6.25) > EASA $_{G\text{-}EX}$ (3.09) > EASA $_{G\text{-}ST}$ (2.69) > EASA $_{G\text{-}EX\text{-}300}$ (2.12)

References

1 Q. Han, Z. Cheng, J. Gao, Y. Zhao, Z. Zhang, L. Dai and L. Qu, *Adv. Funct. Mater.*, 2017, **27**, 1606352.

2 Y. Zheng, Y. Jiao, Y. Zhu, L. H. Li, Y. Han, Y. Chen, A. Du, M. Jaroniec and S. Z. Qiao, *Nat.*

Commun., 2014, **5**, 3783.

3 J. Duan, S. Chen, M. Jaroniec and S. Z. Qiao, *ACS Nano*, 2015, **9**, 931–940.

4 L. Wei, H. E. Karahan, K. Goh, W. Jiang, D. Yu, Ö. Birer, R. Jiang and Y. Chen, *J. Mater. Chem. A*, 2015, **3**, 7210–7214.

5 X. Yan, Y. Jia, T. Odedairo, X. Zhao, Z. Jin, Z. Zhu and X. Yao, *Chem. Commun.*, 2016, **52**, 8156–8159.

6 F. Davodi, M. Tavakkoli, J. Lahtinen and T. Kallio, *J. Catal.*, 2017, **353**, 19–27.

7 Y. Jia, L. Zhang, A. Du, G. Gao, J. Chen, X. Yan, C. L. Brown and X. Yao, *Adv. Mater.*, 2016, **28**, 9532–9538.

8 J. Lai, S. Li, F. Wu, M. Saqib, R. Luque and G. Xu, *Energy Environ. Sci.*, 2016, **9**, 1210–1214.

9 N. Cheng, Q. Liu, J. Tian, Y. Xue, A. M. Asiri, H. Jiang, Y. He and X. Sun, *Chem. Commun.*, 2015, **51**, 1616–1619.

10 T. Y. Ma, S. Dai, M. Jaroniec and S. Z. Qiao, *Angew. Chemie - Int. Ed.*, 2014, **53**, 7281–7285.

11 Z. Liu, Z. Zhao, Y. Wang, S. Dou, D. Yan, D. Liu, Z. Xia and S. Wang, *Adv. Mater.*, 2017, **29**, 1606207.

12 J. Zhang, Z. Zhao, Z. Xia and L. Dai, *Nat. Nanotechnol.*, 2015, **10**, 444–452.

13 N. Jia, Q. Weng, Y. Shi, X. Shi, X. Chen, P. Chen, Z. An and Y. Chen, *Nano Res.*, 2018, **11**, 1905–1916.

14 Y. Zhao, R. Nakamura, K. Kamiya, S. Nakanishi and K. Hashimoto, *Nat. Commun.*, 2013, **4**, 2390.